

Silicon nanowires with controlled sidewall profile and roughness fabricated by thin-film dewetting and metal-assisted chemical etching

This article has been downloaded from IOPscience. Please scroll down to see the full text article.

2013 Nanotechnology 24 225305

(<http://iopscience.iop.org/0957-4484/24/22/225305>)

View [the table of contents for this issue](#), or go to the [journal homepage](#) for more

Download details:

IP Address: 192.17.144.50

The article was downloaded on 07/05/2013 at 05:37

Please note that [terms and conditions apply](#).

Silicon nanowires with controlled sidewall profile and roughness fabricated by thin-film dewetting and metal-assisted chemical etching

B P Azeredo¹, J Sadhu¹, J Ma¹, K Jacobs¹, J Kim¹, K Lee¹, J H Eraker², X Li³, S Sinha¹, N Fang⁴, P Ferreira¹ and K Hsu¹

¹ Mechanical Science and Engineering, University of Illinois at Urbana-Champaign, 1206 West Green Street, Urbana, IL 61801, USA

² Ball Aerospace and Technology Corp., Boulder, CO 80301, USA

³ Electrical and Computer Engineering, University of Illinois at Urbana-Champaign, 1406 West Green Street, Urbana, IL 61801, USA

⁴ Mechanical Engineering, Massachusetts Institute of Technology, 77 Massachusetts Avenue, Cambridge, MA 02139, USA

E-mail: pferreir@illinois.edu and khsu5@illinois.edu

Received 24 January 2013, in final form 3 April 2013

Published 3 May 2013

Online at stacks.iop.org/Nano/24/225305

Abstract

This paper presents a non-lithographic approach to generate wafer-scale single crystal silicon nanowires (SiNWs) with controlled sidewall profile and surface morphology. The approach begins with silver (Ag) thin-film thermal dewetting, gold (Au) deposition and lift-off to generate a large-scale Au mesh on Si substrates. This is followed by metal-assisted chemical etching (MacEtch), where the Au mesh serves as a catalyst to produce arrays of smooth Si nanowires with tunable taper up to 13°. The mean diameter of the thus fabricated SiNWs can be controlled to range from 62 to 300 nm with standard deviations as small as 13.6 nm, and the areal coverage of the wire arrays can be up to 46%. Control of the mean wire diameter is achieved by controlling the pore diameter of the metallic mesh which is, in turn, controlled by adjusting the initial thin-film thickness and deposition rate. To control the wire surface morphology, a post-fabrication roughening step is added to the approach. This step uses Au nanoparticles and slow-rate MacEtch to produce rms surface roughness up to 3.6 nm.

[S] Online supplementary data available from stacks.iop.org/Nano/24/225305/mmedia

(Some figures may appear in colour only in the online journal)

1. Introduction

Self-assembled patterns have been increasingly integrated into bottom-up and top-down semiconductor fabrication approaches due to their high-resolution and avoidance of expensive lithographic processes. These integrated approaches have allowed new designs of a wide range of novel structures such as silicon nanowire (SiNW) arrays for applications in nanostructured thermoelectric devices [1], high-emissivity

surfaces [2] and high-capacity Li-ion battery anodes [3]. Substantial work has gone into improving the resolution [4] and aspect ratio [5], and to controlling the geometry [6] and morphology [7] of these 1D semiconductor nanostructures. One specific example is the thermoelectric effect in rough SiNWs. As the diameter of the SiNWs decreases and their surface roughness increases, they exhibit a near-unity thermoelectric figure of merit at room temperature. This is due to the confinement and boundary scattering of phonons

traveling in the SiNWs [8]. Another example appears in the optical properties of a SiNW forest. High-aspect ratio, tapered SiNWs [2] allow for near black-body behavior due to the smooth transition in the refractive index and photon trapping. Thus, scalable and economic manufacturing strategies may enable the deployment of such devices in commercial applications.

As alluded to earlier, self-assembly methods can be combined with several fabrication techniques—including deep reactive ion etching (DRIE), metal-assisted chemical etching (MacEtch) [9] or vapor–liquid–solid (VLS) growth [10, 11]—to create 1D Si structures. In this context, self-assembly is used to either directly or indirectly (by patterning a mask) pattern the catalyst for the process. An example of directly forming a forest of 1D silicon nanotips was first investigated by Jansen *et al*, using reactive ion etching (RIE) on a silicon wafer. The redeposition of polymer masks and adsorption of silicon dioxide particles during the etching step in RIE create micromasks that protect the substrate to form silicon tips (also known as micrograss). The taper profile of these structures was controlled by adjusting the pressure, flow of reactive gases and power of the RIE process [12]. In a single-step, this process can both (1) create the mask for nucleating the tips, and (2) etch the substrate, creating high-aspect ratio, tapered, and dense arrays of nanotips. More recently, other plasma etching techniques have been developed to yield more robust results for controlling the taper and creating self-masks with higher densities, such as pulsed-mode DRIE [13] and electron cyclotron resonance plasma etching [2], respectively. While these approaches are economical and yield samples with low reflectivity in the visible and near-IR range, little work has been carried out to independently adjust the taper and the density of self-masked patterns, which may allow for further reduction in reflectivity.

A typical example of indirectly patterning the catalyst uses dip coating with a monolayer of silica beads [14], which uses the Langmuir–Blodgett assembly method [15, 16] to produce a close-packed layer of beads over a large area [17, 6]. This step is followed by an isotropic RIE step to separate and shrink the beads, starting from a 200–600 nm diameter [6]. Used as a mask over which a thin metal film is deposited, a metallic mesh with monodispersed pores is produced by the removal or lift-off of the beads. This, in turn, is used as a catalyst by the MacEtch process to produce SiNW arrays [15]. As-fabricated wires can be shrunk to 60–120 nm by thermal oxide growth and removed by etching in hydrofluoric acid. However, this approach suffers from the drawback of producing SiNW forests with low areal coverage, detrimental for system-level efficiency of several of the applications previously discussed.

Porous anodized aluminum oxide (AAO) [18] with monodispersed pores has also been used to produce SiNWs, with the advantage of having highly tunable diameter control in the sub-200 nm range. AAO is grown on a bulk aluminum foil [19, 20] or thin-film [21] by a two-step anodization with the pore depth and size controlled by the anodization time and the pore opening step. Multiple approaches [6, 21, 19] may be used to open up the bottoms of the pores so that the membrane

can be used as a template. The AAO membrane is manually transferred to the silicon substrate with the use of a polymeric film as a handle after the Al substrate is etched away [19]. The polymer handle is then removed by dissolving in a solvent. AAO membranes—transferred via this method—are covered with a Au film and immersed in MacEtch solution to produce SiNWs. Even though this process integration has been shown to produce SiNW arrays, the areal coverage of SiNWs produced by this method is limited by the template wall thickness and pore closure effects [19, 20]. Moreover, the process requires a number of delicate manual steps in the transfer of the template, thus limiting the size of the patterned surface and the yield.

Thin-film dewetting is a scalable and robust process for the creation of self-assembled monolayers of metal nanoparticles in the 10–500 nm size range on oxide surfaces [7, 22]. A metallic thin-film is first deposited on the substrate. This is followed by a thermal annealing step that activates thermal grooving in the thin-film and results in the formation of individual nanoparticles. Unlike approaches that use AAO templates or dip coating and are capable of producing monodispersed metal particles for MacEtch, this process inherently creates particles with a size distribution with a standard deviation starting at 5 nm for sub-20 nm particles and growing up to 40 nm for 150 nm particles. The dewetting behavior has been shown to spontaneously occur for metals such as Ag [22], Co [23], Ni [24, 25], Cu [26], Au [27], and Pt [28]. The annealing temperature to cause dewetting is usually less than a third of the metal's bulk melting temperature. Accelerated diffusion of impurities into semiconductors at elevated temperatures limits the use of high-melting point metals. Low-temperature options include Ag, Au, Co, and Ni, which typically exhibit dewetting behavior between 300 °C and 600 °C.

Metal-assisted chemical etching is a process in which a mixture of HF and an oxidant (typically H₂O₂) is used to etch a semiconductor such as Si in the presence of metal [29]. The process works by injecting a hole into the semiconductor from the reduction of an oxidant at the metal–solution interface. Then, the availability of holes in the vicinity of the semiconductor–metal interface triggers a reaction between the surface silicon atoms and the hydrofluoric acid through one of the proposed diffusion mechanisms in the literature [30]. The balance between hole injection and consumption maintains holes localized at the metal–substrate interface and, consequently, directional etching is achieved with non-porous single crystalline features being generated. When deployed in SiNW fabrication, MacEtch produces nanowires with aspect ratios greater than 100 [5], provided the diffusion of reactants and products to and from the reaction zone is abundant. For this reason, MacEtch has been widely used for the generation of dense and vertically aligned nanowires for integration with planar manufacturing processes [31].

In regards to morphology control of SiNWs, MacEtch has been demonstrated to achieve some roughness control of the sidewall profile by increasing the ratio of the oxidizer concentration to that of the HF [7] and by changing the

catalyst metal [32]. Increased oxidizing activity produces excess holes which are injected into the Si and transported to the SiNW boundary. The presence of holes at the SiNW surface as it is formed makes it susceptible to HF and causes roughening of the surface of the nanowire. Our previous work [7] shows that RMS roughness can be controlled only in the 0.5–2 nm range. After 2 nm, the wire roughening becomes so aggressive that it results in the formation of porous SiNWs, significantly reducing their electrical conductivity. The same mechanism for roughness generation can also be used for tuning the taper of its sidewall. For instance, further increasing the oxidizing activity accelerates the sidewall porous formation and its subsequent dissolution in HF. This results in a tapered external profile [33]. This approach, unfortunately, also causes the core of the SiNW to be porous for most levels of useful tapering.

In this paper, we report a fabrication scheme to obtain SiNW arrays with controlled sidewall morphology, size distribution and density. Our approach combines the dewetting process with MacEtch through image reversal by a lift-off process that converts Ag particle patterns into a Au mesh pattern. By fine control of the deposition rate and thickness of the evaporated Ag film that is dewetting into Ag nanoparticles, SiNW arrays with average diameter as small as 61 nm with a standard deviation of 13 nm are produced. Further, it is shown that, by altering the chemical composition of the MacEtch solution, tapered wires are also produced, with application to broadband anti-reflection surfaces. This paper also develops an approach to produce SiNWs with surface roughness fine-tuned in the 0.5–3.5 nm range consistently across the wire length. To accomplish this, an additional post-roughening step is used. As-formed SiNWs are coated with Au nanoparticles via sputtering and etched by MacEtch again. Au nanoparticles etch toward the core of SiNWs. Roughness control is obtained by controlling the etching time. After roughening, the SiNW surface develops a native oxide and the Si/SiO₂ interface roughness is characterized by TEM. This work may enable a deeper understanding of the relationship between roughness and thermal conductivity of SiNWs, and can potentially be implemented in large-scale manufacturing of SiNW thermoelectric devices. It also provides an affordable and scalable pathway for the manufacture of large-area, high-emissivity surfaces for stray light reduction in telescopes.

2. Silicon nanowire fabrication

Two sets of samples were manufactured for the purpose of investigating the roughness dependence on MacEtch parameters and the broadband anti-reflective properties of tapered SiNWs. The first set comprised of smooth SiNWs with average diameter in the 110–140 nm range that were roughened to various levels and analyzed under TEM. The second set comprised of as-doped and post-doped tapered SiNWs with average diameter around 300 nm.

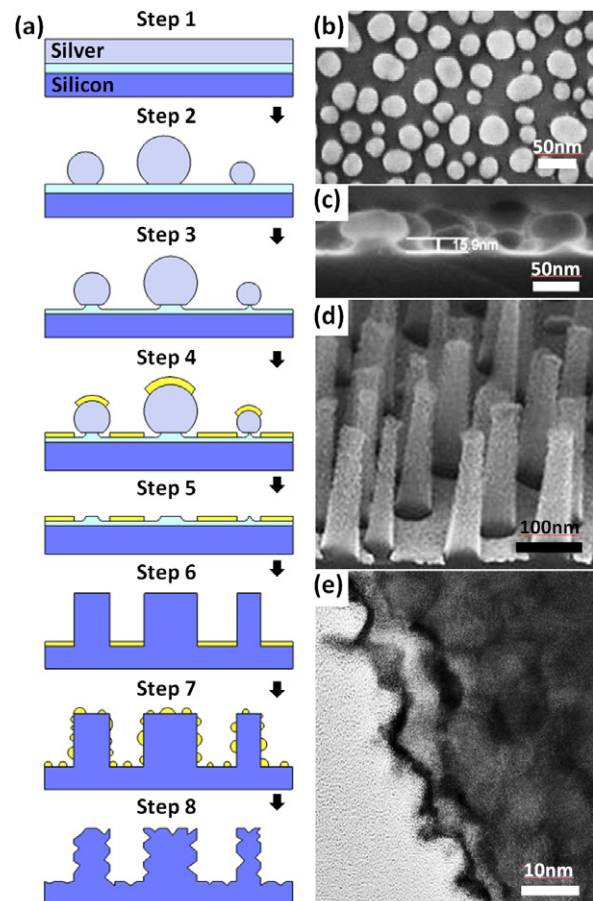


Figure 1. (a) Fabrication overview: silver films are evaporated onto a clean 15 nm thick thermally grown SiO₂ surface at controlled deposition rate and thickness (step 1) (b), thin-films are annealed in vacuum, breaking into individual particles (step 2), sub-120 nm Ag particles are undercut with BOE to increase their height and facilitate lift-off (step 3) (c), a thin Au catalyst layer is evaporated (step 4), Ag nanoparticles are etched away at room temperature with silver etchant solution (step 5), MacEtch at different ethanol concentrations produces straight and tapered SiNWs (step 6) (d), and Au nanoparticles are sputtered (step 7) and etched in diluted MacEtch solution to generate surface roughness (step 8) (e).

2.1. Particle size control via dewetting parameters

The process begins by growing a 15 nm oxide layer on degreased and RCA-1 cleaned (100) Si wafers (1–10 Ω cm) in a Lindberg Hevi-Duty Lancer M-300 tube furnace at 1000 °C for 13 min with a 4 sccm pure oxygen flow rate. Subsequently, silver deposition is performed in a Temescal e-beam evaporation system with thickness and deposition rate monitored by a quartz crystal monitor (figure 1(a): step 1). The silver films are then annealed at 350 °C in a rapid thermal annealing chamber that focuses an infrared light source on the sample (model SSA-P610C, manufactured by ULVAC-RIKO, Inc.) for 4 h at $3\text{--}8 \times 10^{-7}$ Torr (figure 1(a): step 2); at the end of this step, the Ag film is fully dewetted into isolated particles (figure 1(b)). For sub-100 nm particles, we use scanning electron microscopy (SEM) to characterize the particle size distribution as a function of the deposition thickness at a deposition rate as low as 0.1 \AA s^{-1} . The

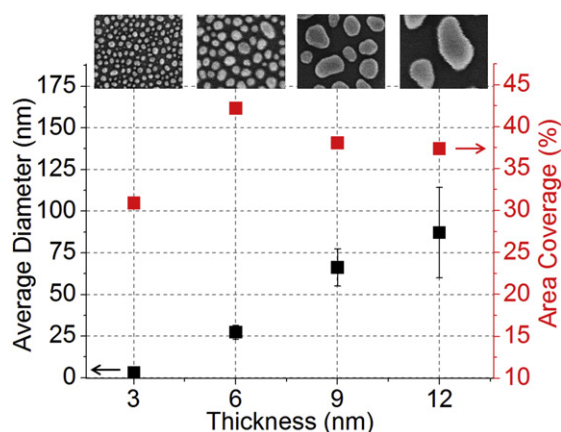


Figure 2. Characterization of sub-100 nm average Ag particle size: average diameter (black; error bars represent one standard deviation of the wire diameter distribution) and area coverage (red) as a function of film thickness at constant 0.1 \AA s^{-1} . The SEM images at the top represent each data point at the same magnification.

SEM data are analyzed with ImageJ (see supplementary figure 1 available at stacks.iop.org/Nano/24/225305/mmedia) and results for the average particle diameter and areal coverage are shown in figure 2 as a function of the deposition parameters. The parameters for the 100–400 nm particle size range were reproduced from previous studies [22].

The samples are immersed in a buffered oxide etch ($\text{HF}:\text{NH}_4\text{F} = 6:1; \text{v}:\text{v}$) for 20 s in an ice bath with the temperature kept at 0°C with constant agitation (figure 1(a): step 3). This step undercuts the oxide film under the silver particles and facilitates the subsequent lift-off process (figure 1(c)). Theoretically, 1% HF could also be used to achieve an even slower undercut rate [34]. This is particularly important for sub-120 nm particles and unnecessary otherwise (see supplemental figure 2 available at stacks.iop.org/Nano/24/225305/mmedia). Next, all samples are evaporated with 10 nm Au at 0.5 \AA s^{-1} in the same e-beam evaporation system (figure 1(a): step 4), immersed in an etchant solution ($\text{NH}_4\text{OH}:\text{H}_2\text{O}_2:\text{methanol} = 1:1:2; \text{v}:\text{v}:\text{v}$) at room temperature and sonicated four times for 10 min in each round. After sonication in RCA-1, most silver nanoparticles covered with Au have been etched (figure 1(a): step 5), leaving behind a gold mesh pattern on the substrate. The gold mesh is now used as the catalyst template for MacEtch (figure 1(a): step 6).

2.2. MacEtch: straight versus tapered wires

The Si substrates with the patterned Au mesh are etched in MacEtch to produce straight ($\text{HF}(49\%):\text{H}_2\text{O}_2(30\%):\text{ethanol} = 13:2:19; \text{v}:\text{v}:\text{v}$) and tapered ($\text{HF}(49\%):\text{H}_2\text{O}_2(30\%):\text{ethanol} = 13:2:\text{X}; \text{v}:\text{v}:\text{v}$) SiNWs (figure 1(d)), in which 'X' represents the volume ratio of 99.9% ethanol added to the mixture. For this work, solutions are always made freshly before each experiment and used immediately within 10 min. To understand the effect of ethanol concentration on taper formation, the volume ratio of ethanol (X) was varied from 56 to 110 at a fixed 13:2 volumetric ratio of HF(49%) and

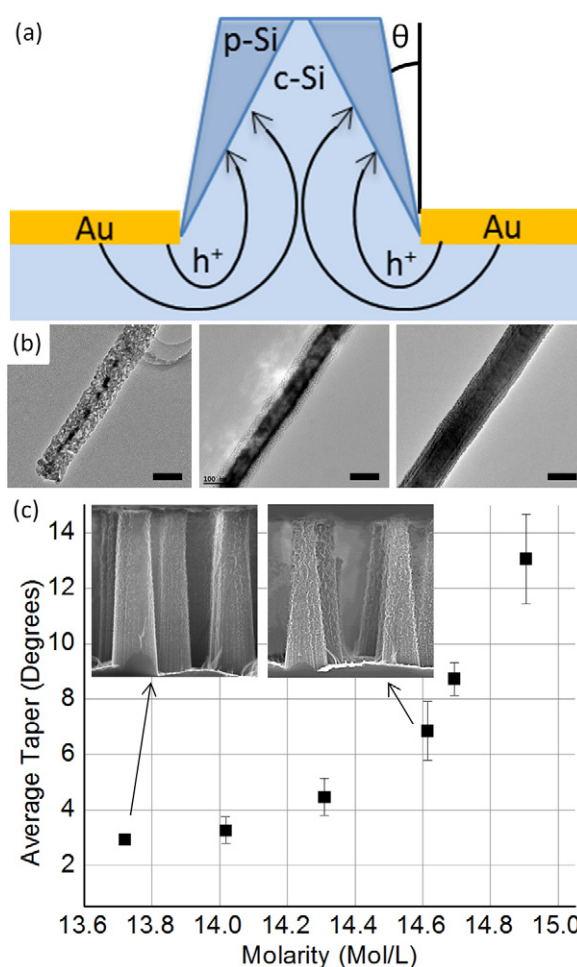


Figure 3. Taper control: (a) schematics of hole diffusion and migration toward the SiNW shell surface, showing the external angle, θ , (b) TEM images of the tip to the base (from left to right, respectively) of a SiNW etched in MacEtch in $[\text{EtOH}] = 13.4 \text{ M}$, (c) dependence of taper angle on ethanol molarity in solution. The scale bars are 100 nm in length.

$\text{H}_2\text{O}_2(30\%)$. Samples were cleaved and we studied their cross-sections in an SEM, measuring the taper of the wires produced. The taper of the wires is constant throughout its height for all cases, which indicates that the local rates of hole injection and consumption are constant. This observation leads to the conclusion that the concentration of the reactants does not decay during the etching. Additionally, MacEtch etch rates are reported to be constant for several hours in other papers [29]. From the analysis of the SEM data, we found that the external taper angle of SiNWs increases for solutions with higher ethanol concentration, and detailed information is shown in figure 3 (see supplementary figure 3 available at stacks.iop.org/Nano/24/225305/mmedia). After MacEtch, the Au mesh is removed by an etch step with aqua regia for 90 s.

2.3. SiNW roughening

Au nanoparticles were deposited on a set of straight SiNW samples $1 \mu\text{m}$ long with average diameter between 110 and 140 nm by sputtering on a Denton Desk II TSC (the power

was set at 20% for 15 s). All-angle rotation was activated to uniformly coat the nanowire surfaces (figure 1(a): step 7). At that point, the samples were cleaved into 1 cm² pieces and the SiNWs were roughened (figure 1(a): step 8) by a second etch step that involved immersing the samples in dilute MacEtch solution (HF(49%):H₂O₂(30%):H₂O = 1:1:24; v:v:v) for different amounts of time, ranging from 5 to 25 s. The sidewall roughness of the samples was characterized by high-resolution transmission electron microscopy (HRTEM) (figure 1(e)) and the RMS roughness is plotted as a function of the duration of the roughening etch step (figure 4(a)) shown in step 8 of figure 1(a). High-resolution images of the Si/SiO₂ boundary are obtained by tilting the nanowire to [110] zone-axis angstrom level resolution. Several HRTEM images recorded continuously along the length of a nanowire are seamlessly stitched together to generate the roughness profile of the nanowire over a length of ~500 nm. This procedure was conducted for three nanowires from each array to obtain an average RMS roughness for each sample.

2.4. Tapered SiNWs for anti-reflection measurements

To investigate light reflection, two sets of straight and tapered SiNWs samples with a 300 nm average diameter were fabricated using MacEtch. Tapered samples were made with 13.4 mol l⁻¹ ethanol concentration. The first set contained wires that were straight and tapered with lengths of 2 μm and 1.5 μm, respectively. For the second set, tapered wires with lengths set at 11 μm were boron doped in a diffusion chamber with a boron diffusion source (BN-975, Saint-Gobain Ceramics) for 40 min at temperatures of 900 and 1000 °C. The reflectivity in the visible and near-IR range of the first (figure 5(a)) and second (figure 5(b)) sets was obtained in a Cary 5000 spectrophotometer.

3. Results and discussion

3.1. SiNW fabrication and taper control

We have shown that dewetting of a Ag thin-film can result in nanoparticles with diameters in the size range of 10–80 nm and with area coverage in the 32–42% range. This is related to the changes in thin-film nucleation and growth kinetics as a result of selecting a deposition rate as well as film thickness [22]. The nucleation process during evaporation produces peaks and valleys on the thin-film top surface, centered at the nucleation sites and the mid-points between them, respectively. These peaks and valleys on the film surface serve as the initial conditions for dewetting upon exposure of the film to elevated temperatures. The initial shape favors thermal grooving in the valley region (grain boundary), resulting in the formation of particles centered at their nucleation sites. For a given temperature cycle, the nucleation density for silver island formation on a substrate during dewetting remains the same as that of silver grain formation during deposition. This is shown to be inversely proportional to the incoming flux of atoms during deposition [22]. This allows us to obtain high area coverage (particle density)

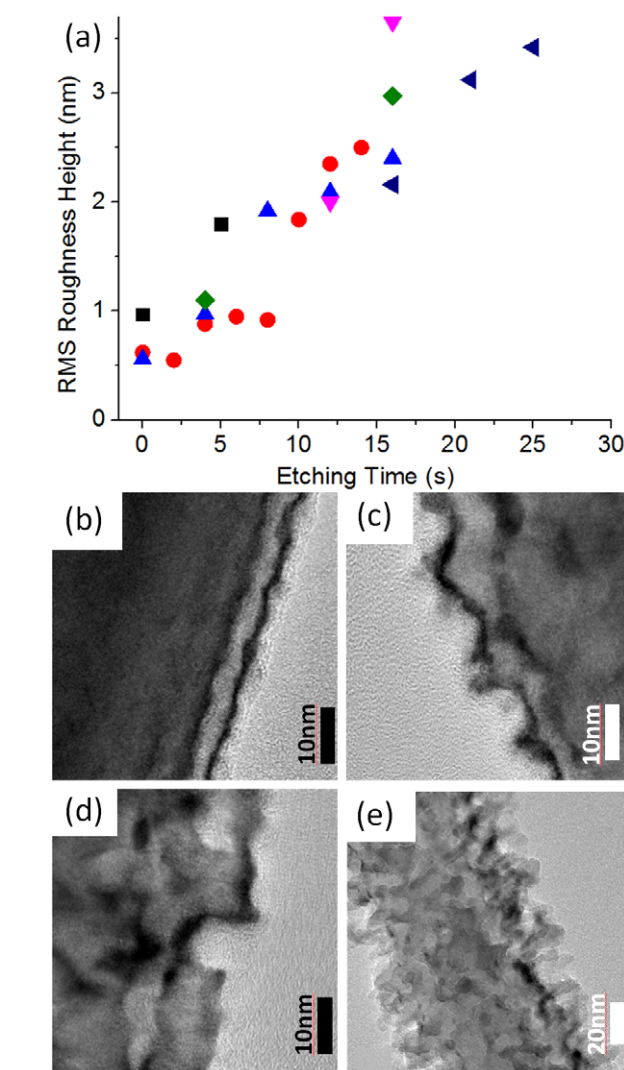


Figure 4. Post-roughening characterization. (a) RMS height as a function of roughening time in diluted MacEtch solution. Low-magnification TEM images of SiNWs (b) as-prepared, and after (c) 5 s, (d) 10 s, and (e) 20 s of roughening.

at low evaporation rates (figure 2). In the same figure, the average diameter increases with thickness and we observe a peak in the area coverage. This slight decrease in area coverage as the deposition thickness increases is due to merged grains during dewetting. This is possible because the thermal grooving process becomes less efficient at completely separating nucleation sites as the film thickness increases. This also causes the resulting particles to lose their circular shape, and the resulting particle density to decrease.

In the fabrication process, the limiting step for producing SiNWs from the dewetted sub-100 nm Ag particles via MacEtch is the metal lift-off technique described in section 2.1. For this regime, the particle height is small and less than twice the Au film thickness (see supplementary figure 2 available at stacks.iop.org/Nano/24/225305/mmedia). Therefore, many particles are coated by Au resulting in a low lift-off yield. To address this issue, we use a BOE (buffered oxide etch) step to etch the oxide layer that was deposited

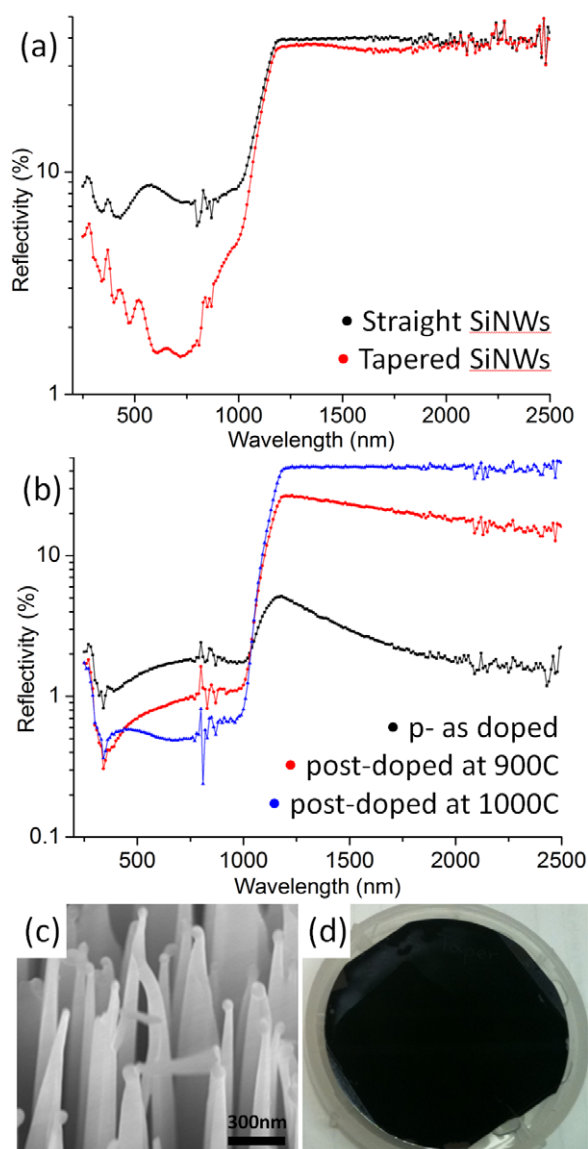


Figure 5. Reflectivity of (a) straight 2 μm long (black) and tapered 1.5 μm long (red) SiNWs and (b) of tapered 11 μm long SiNWs with different doping conditions: 1–10 Ω p-type (reference, blue), post-doped at 900 $^{\circ}\text{C}$ for 35 min (red), post-doped at 1000 $^{\circ}\text{C}$ for 35 min; instrumental noise was significant at 800–900 nm and 2000–2500 nm but did not obscure the data trend. (c) SEM of post-doped SiNWs post-doped at 1000 $^{\circ}\text{C}$. (d) Photograph of a sample fabricated on a 2 in wafer.

before the Ag film. This increases the height of the particles by an additional 10–15 nm and also undercuts the oxide under the silver particles to produce pedestal-like structures that greatly facilitate the lift-off process. The smallest reproducible average diameters over 1 cm^2 samples were 61 nm at 22% area coverage and 67 nm at 46% area coverage (see supplementary table 1 available at stacks.iop.org/Nano/24/225305/mmedia). Further improvements such as decreasing the Au grain size and its thickness are being investigated to fine tune the lift-off yield for even smaller diameters.

Silicon wire tapering is possible by addition of ethanol and changing its concentration in the MacEtch solution. The

flux of holes injected into the band structure of Si is generated by the H_2O_2 reduction at the Au–MacEtch solution interface (cathode). When excess holes—not consumed by the anodic Si etch reaction at the Si–Au interface—become available, they migrate away from the Si–Au interface, toward the rest of the Si surface exposed to the etchant. The presence of excess holes in the Si near the surfaces of the wires increases the rate of SiO_2 formation at the surface. This is subsequently etched by HF [33] to create a porous Si layer. Continuation of this process results in growth of the pores, loss of the outer surface layer, and migration of the porous layer toward the center of the wires. The tips of the wires, having been created first, are subjected to this process for the longest time, and hence the wires develop a taper. The thickness of the porous Si layer on the already formed wires increases monotonically with time. As a result of this, the tips of the nanowires have a thicker porous layer as compared to the bottoms of the wires (figures 3(a) and (b)). A similar observation has been made by Chartier *et al* [33]. In their study of Si MacEtch with Au nanoparticles as catalysts, they found that decreasing the molar concentration of HF relative to H_2O_2 produces a porous tapered sidewall. The characterization of the external taper angle versus ethanol concentration is shown in figure 3(c). While the addition of ethanol can create controllable wire tapering, this effect was not observed when water was used instead of ethanol.

As described earlier, when excess holes become available, the process described above can result in tapered SiNWs. From the perspective of the overall reaction [29], excess holes can become available by two means: an increase in hole generation on the cathode (Au–etchant interface) or a decrease in the rate at which holes are consumed on the anode (Au–Si interface). Our observations indicate that while the water addition reduces the kinetic rates of the cathode and anode reactions equally, the addition of ethanol only reduces the hole consumption rate on the anode. As a result of this, the excess amount of holes can migrate from the anode (Au–Si interface).

3.2. TEM characterization of roughness dependence on etching time

In the roughening approach, the catalyst is composed of Au nanoparticles that penetrate a few nanometers into the core direction of the nanowires etching a variety of crystallographic planes toward the SiNW core, causing reformation of the Si and SiO_2 surfaces (figure 4). Since the penetration path is small, we do not observe any coherence or preferred crystallographic direction in the etching performed by the nanoparticles. TEM imaging followed by image analysis reveals the longitudinal topography and surface roughness of the nanowires and the Si and SiO_2 interface. Control over RMS roughness height is attained in the 0.5–3.5 nm range by controlling the etch time (figure 4(a)). Such fine control is achieved as a result of the substantial reduction in MacEtch rate, made possible by water dilution (see supplementary figure 4 available at stacks.iop.org/Nano/24/225305/mmedia).

3.3. Anti-reflective properties of tapered and doped SiNWs

We first compare the reflectivity characteristics of straight and tapered structures in the visible and near-IR range. The effect of a slightly tapered SiNW is captured in figure 5(a). The smooth transition in the refractive index derived from tapered nanowires reduces the reflectivity in the visible range by 77% (particularly around a wavelength of 700 nm) relative to straight nanowires for samples with similar lengths. This is possible due to the subwavelength scale of the SiNWs. In the visible range, the reflectivity spectrum for the tapered SiNW agrees well with studies on anti-reflection of silicon nanotips of equivalent length [2]. Beyond the band gap wavelength, light travels into the sample and it is not well absorbed due to the low absorption coefficient of low-doped Si. As a result, light is reflected from the back of the wafer and, thus, we observe a jump in reflectivity.

Increasing absorption in the near-IR becomes fundamental to reducing reflectivity in this range. One approach is to increase the doping level. Higher doping concentrations facilitate phonon-assisted absorption around the band gap wavelength [35, 36] and increase the free carrier density [37]. Both of these effects contribute to lowering the reflectivity in our measurements. Figure 5(b) shows the effect of doping on anti-reflection of tapered SiNWs as a function of the temperature in which the boron doping was carried out.

4. Conclusion

A novel manufacturing pathway to obtain SiNWs with tunable taper angle and sidewall roughness is presented. The process of integration of metal dewetting and MacEtch produces wire diameters that are ideal for making anti-reflection surfaces and exploring phonon confinement. The roughening of the side walls provides an additional design parameter in thermoelectric devices to potentially increase the boundary scattering of phonons. Taper control enables significant reduction of the reflectivity of SiNWs creating high-aspect ratio nanostructures and ideal high-emissivity surfaces in the visible and near-IR range with the incorporation of post-doping.

Acknowledgments

The authors acknowledge financial support for this work from the National Science Foundation (Grant No. 0749028 CMMI) through the Center for Nanoscale Chemical-Electrical-Mechanical Manufacturing Systems (NanoCEMMS) at the University of Illinois and the Advanced Research Project Agency—Energy, Department of Energy (Grant No. DOEDE-AR-0000041PF-ARRA). The work was carried out in part at the Frederick Seitz Materials Research Laboratory Central Facilities, University of Illinois.

References

[1] Hochbaum A I, Chen R, Delgado R D, Liang W, Garnett E, Najarian M, Majumdar A and Yang P 2008 Enhanced

- thermoelectric performance of rough silicon nanowires *Nature* **451** 136–67
- [2] Huang Y *et al* 2007 Improved broadband and quasi-omnidirectional anti-reflection properties with biomimetic silicon nanostructures *Nature Nanotechnol.* **2** 770–4
- [3] Chan C K, Peng H N, Liu G, McIlwrath K, Zhang X F, Huggins R A and Cui Y 2008 High-performance lithium battery anodes using silicon nanowires *Nature Nanotechnol.* **3** 31–5
- [4] Wang C, Murhpy P, Yao N, McIlwrath K and Chou S 2011 Growth of straight silicon nanowires on amorphous substrates with uniform diameter, length, orientation, and location using nanopatterned host-mediated catalyst *Nano Lett.* **11** 5247–51
- [5] Balasundaram K, Sadhu J S, Shin J C, Azeredo B P, Chanda D, Malik M, Rogers J A, Ferreira P, Sinha S and Li X 2012 Porosity control in metal assisted chemical etching of degenerately doped silicon nanowires *Nanotechnology* **23** 305304
- [6] Hsu C, Connor S, Tang M and Cui Y 2008 Wafer-scale silicon nanopillars and nanocones by Langmuir–Blodgett assembly and etching *Appl. Phys. Lett.* **93** 133109
- [7] Azeredo B P, Hsu K, Ma J, Tong T, Oh D, Seong M, Sinha S, Cahill D, Ferreira P and Fang N 2011 Introducing side-wall roughness through control of hole injection during metal-assisted chemical etching of Si nanowire arrays for reduced thermal conductivity *Materials Research Symp. (San Francisco)*
- [8] Boukai A I, Bunimovich Y, Tahir-Kheli J, Yu J, Goddard W and Heath J R 2008 Silicon nanowires as efficient thermoelectric materials *Nature* **451** 168–71
- [9] Li X and Bohn P W 2000 Metal-assisted chemical etching in HF/H₂O₂ produces porous silicon *Appl. Phys. Lett.* **77** 2572
- [10] Koren E, Hyun J K, Givan U, Hemesath E R, Lauhon L J and Rosenwaks Y 2011 Obtaining uniform dopant distributions in VLS-grown Si nanowires *Nano Lett.* **11** 183–7
- [11] Allen J *et al* 2008 High-resolution detection of Au catalyst atoms in Si nanowires *Nature Nanotechnol.* **3** 168–73
- [12] Jansen H, Boer M, Legtenberg R and Elwenspoek M 1995 The black silicon method: a universal method for determining the parameter setting of a fluorine-based reactive ion etcher in deep silicon trench etching with profile control *J. Micromech. Microeng.* **5** 115–20
- [13] Jansen H V, Boer M J, Innikrishnan S, Louwse M C and Elwenspoek M C 2009 Black silicon method X: a review on high speed and selective plasma etching of silicon with profile control: an in-depth comparison between Bosch and cryostat DRIE processes as a roadmap to next generation equipment *J. Micromech. Microeng.* **19** 033001
- [14] Bogush G H, Tracy M A and Zukoski C F 1988 Preparation of monodisperse silica particles: control of size and mass fraction *J. Non-Cryst. Solids* **104** 95–106
- [15] Peng K, Zhang M, Lu A, Wong N, Zhang R and Lee S 2007 Ordered silicon nanowire arrays via nanosphere lithography and metalinduced etching *Appl. Phys. Lett.* **90** 163123
- [16] Bardosova M, Pemble M, Povey I and Tredgold R 2010 The Langmuir–Blodgett approach to making colloidal photonic crystals from silica spheres *Adv. Mater.* **22** 3104–24
- [17] Garnett E and Yang P 2010 Light trapping in silicon nanowires solar cells *Nano Lett.* **10** 1082–7
- [18] Masuda H and Fukuda K 1995 Ordered metal nanohole arrays made by a two-step replication of honeycomb structures of anodic alumina *Science* **268** 1466–8
- [19] Hong J, Kim K, Kwon N, Lee J, Whang D and Chung I 2010 Fabrication of vertically aligned silicon nanowires on Si(100) substrates utilizing metal-assisted etching *J. Vac. Sci. Technol. A* **28** 734–40

- [20] Lei Y and Chim W 2005 Shape and size control of regularly arrayed nanodots fabricated using ultrathin alumina masks *Chem. Mater.* **17** 580–5
- [21] Huang Z, Zhang X, Reiche M, Liu L, Lee E, Shimizu T, Senz S and Gosele U 2008 Extended arrays of vertically aligned sub-10 nm diameter [100] Si nanowires by metal-assisted chemical etching *Nano Lett.* **8** 3046–51
- [22] Oates T W H and Sugime H 2009 Combinatorial surface-enhanced Raman spectroscopy and spectroscopic ellipsometry of silver island films *J. Phys. Chem. C* **113** 4820–8
- [23] Oh Y, Ross C A, Jung Y S, Wang Y and Thompson C V 2009 Cobalt nanoparticle arrays made by templated solid-state dewetting *Small* **5** 860–5
- [24] Randolph S J, Fowlkes J D, Melechko A V, Klein K L, Meyer H M, Simpson M L and Rack P D 2007 Controlling thin film structure for the dewetting of catalyst nanoparticle arrays for subsequent carbon nanofiber growth *Nanotechnology* **18** 465304
- [25] Lee P and Chang C 2007 Spectroscopic characterization of Ni films on sub-10 nm silica layers: thermal metamorphosis and chemical bonding *Surf. Sci.* **601** 362–75
- [26] Li S, Lee C and Tseng T 2003 Copper-catalyzed ZnO nanowires on silicon (1 0 0) grown by vapor–liquid–solid process *J. Cryst. Growth* **247** 357–62
- [27] Kojima Y and Kato T 2008 Nanoparticle formation in Au thin films by electron-beam-induced dewetting *Nanotechnology* **19** 255605
- [28] Strobel S, Kirkendall C, Chang J and Berggren K 2010 Sub-10 nm structures on silicon by thermal dewetting of platinum *Nanotechnology* **21** 505301
- [29] Huang Z, Geyer N, Werner P, Boor J and Gosele U 2010 Metal-assisted chemical etching of silicon: a review *Adv. Mater.* **23** 285–308
- [30] Geyer N, Fuhrmann B, Huang Z, Boor J, Leipner H S and Werner P 2012 Model for the mass transport during metal-assisted chemical etching with contiguous metal films as catalyst *J. Phys. Chem. C* **116** 13446–51
- [31] Li X 2012 Metal assisted chemical etching for high aspect ratio nanostructures: a review of characteristics and applications in photovoltaics *Curr. Opin. Solid State Mater. Sci.* **16** 71–81
- [32] Chern W, Hsu K, Chun I, Azeredo B P, Ahmed N, Kim K, Zuo J, Fang N, Ferreira P and Li X 2010 Nonlithographic patterning and metal-assisted chemical etching for manufacturing of tunable light-emitting silicon nanowire arrays *Nano Lett.* **10** 1582–8
- [33] Chartier C, Bastide S and Levy-Clement C 2008 Metal-assisted chemical etching of silicon in HF–H₂O₂ *Electrochim. Acta* **17** 5509–16
- [34] Williams K R and Wasilik M 2003 Etch rates for micromachining processing—part II *J. Microelectromech. Syst.* **12** 761–79
- [35] Wagner J 1983 Photoluminescence and excitation spectroscopy in heavily doped n- and p-type silicon *Phys. Rev. B* **29** 2002–9
- [36] Aw S E, Tan H S and Ong C K 1991 Optical absorption measurements of band-gap shrinkage in moderately and heavily doped silicon *J. Phys.: Condens. Matter* **3** 8213–23
- [37] Schmid P E 1981 Optical absorption in heavily doped silicon *Phys. Rev. B* **23** 5531–6